

Mechanistic Modeling of Carbon Steel Corrosion in a Methyldiethanolamine (MDEA)-Based Carbon Dioxide Capture Process

Yoon-Seok Choi,^{†*} Deli Duan,^{**} Shengli Jiang,^{**} and Srdjan Nešić^{*†}

ABSTRACT

A predictive model was developed for corrosion of carbon steel in carbon dioxide (CO₂)-loaded aqueous methyldiethanolamine (MDEA) systems, based on modeling of thermodynamic equilibria and electrochemical reactions. The concentrations of aqueous carbonic and amine species (CO₂, bicarbonate [HCO₃⁻], carbonate [CO₃²⁻], MDEA, and protonated MDEA [MDEAH⁺]) as well as pH values in the MDEA solution were calculated. The water chemistry model showed a good agreement with experimental data for pH and CO₂ loading, with an improved correlation upon use of activity coefficients. The electrochemical corrosion model was developed by modeling polarization curves based on the given species's concentrations. The required electrochemical parameters (e.g., exchange current densities, Tafel slopes, and reaction orders) for different reactions were determined from experiments conducted in glass cells. Iron oxidative dissolution, HCO₃⁻ reduction, and MDEAH⁺ reduction reactions were implemented to build a comprehensive model for corrosion of carbon steel in an MDEA-CO₂-water (H₂O) environment. The model is applicable to uniform corrosion when no protective films are present. A solid foundation is provided for corrosion model development for other amine-based CO₂ capture processes.

KEY WORDS: carbon capture and storage, carbon dioxide capture, carbon steel, corrosion model, MDEA

Submitted for publication: March 22, 2012. Revised and accepted: September 7, 2012. Preprint available online: January 3, 2013, <http://dx.doi.org/10.5006/0695>.

[†] Corresponding author. E-mail: choiy@ohio.edu.

^{*} Institute for Corrosion and Multiphase Technology, Department of Chemical and Biomolecular Engineering, Ohio University, Athens, OH 45701.

^{**} Institute of Metal Research, Chinese Academy of Sciences, Shenyang, 110016, China.

INTRODUCTION

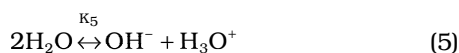
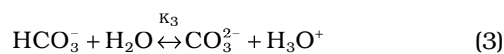
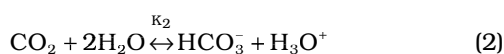
Amine-based carbon dioxide (CO₂) capture process has gained more interest recently as the immediate technological solution that can be used for capturing CO₂ from flue gas streams emitted from coal-fired power plants.¹⁻² Although amine-based CO₂ capture process has been proven in current industrial processes such as natural gas production, syngas scrubbing, etc., the amine process is associated with several technical challenges.³ One of the major problems is corrosion of process components, which results in unexpected downtime, production loss, and even fatalities.

Corrosiveness of an amine solution after CO₂ absorption depends on the type and concentration of amine, CO₂ loading, temperature, solution turbulence, etc.³ From a corrosion standpoint, methyldiethanolamine (MDEA, CH₃N[C₂H₄OH]₂) is the most “forgiving” alkanolamine because it is a tertiary amine and it does not form carbamate (R₃NCOO⁻) with CO₂.⁴⁻⁶ Although there are extensive research data available on corrosion and corrosion inhibition in amine-CO₂ systems,⁷⁻¹² minimal information has been reported in the literature that could aid in establishing a corrosion model for carbon steel in such systems. Veawab and Aroonwilas¹³ reported a mechanistic corrosion model to identify the oxidizing agents responsible for corrosion reactions in the monoethanolamine (MEA [(CH₂)₂OHNH₂]) system. Results indicated that bicarbonate ion and water are the primary oxidizing agents and hydrogen ion played an insignificant role in the reduction reaction.

The objective of the present study was to develop a predictive model for corrosion of carbon steel under operating conditions in the absorber with MDEA related to the CO₂ capture process in fossil fuel-fired power plants.

SPECIATION MODEL FOR A MDEA/CO₂/H₂O SYSTEM

When CO₂ is dissolved and reacted with the MDEA, one can identify eight main species in the solution (MDEA, H₂O, CO₂[aq], MDEAH⁺, bicarbonate ion [HCO₃⁻], carbonic ion [CO₃²⁻], hydronium ion [H₃O⁺], and hydroxide ion [OH⁻]). Carbonic acid (H₂CO₃) is not included here because it has a much lower concentration compared to other carbonic species (HCO₃⁻ and CO₃²⁻) at high pH,¹⁴ and the activity coefficient data for this species were not available in the open literature. The following chemical reactions were considered in the present thermodynamic calculation:¹⁵⁻¹⁷



The reactions shown above can be described by equilibria reactions that can be solved by using the known values of the equilibrium constants (K) to obtain the concentrations of species (c). The equilibrium constants are a function of the temperature and are available in the open literature:¹⁸⁻¹⁹

$$K_1 = \frac{c_{\text{CO}_2}}{p_{\text{CO}_2}} \quad (6)$$

$$K_2 = \frac{c_{\text{HCO}_3^-} c_{\text{H}_3\text{O}^+}}{c_{\text{CO}_2} c_{\text{H}_2\text{O}}^2} \quad (7)$$

$$K_3 = \frac{c_{\text{CO}_3^{2-}} c_{\text{H}_3\text{O}^+}}{c_{\text{HCO}_3^-} c_{\text{H}_2\text{O}}} \quad (8)$$

$$K_4 = \frac{c_{\text{MDEA}} c_{\text{H}_3\text{O}^+}}{c_{\text{MDEAH}^+} c_{\text{H}_2\text{O}}} \quad (9)$$

$$K_5 = \frac{c_{\text{OH}^-} c_{\text{H}_3\text{O}^+}}{c_{\text{H}_2\text{O}}^2} \quad (10)$$

where p_{CO_2} is the partial pressure of CO₂.

Since the solution cannot have a net charge, an electroneutrality equation is:

$$c_{\text{MDEAH}^+} + c_{\text{H}_3\text{O}^+} = c_{\text{HCO}_3^-} + 2c_{\text{CO}_3^{2-}} + c_{\text{OH}^-} \quad (11)$$

In addition, a mass balance can be written for MDEA and carbonic species in the solution:

$$c_{\text{MDEA}} + c_{\text{MDEAH}^+} = \text{constant 1} \quad (12)$$

$$c_{\text{CO}_2} + c_{\text{HCO}_3^-} + c_{\text{CO}_3^{2-}} = \text{constant 2} \quad (13)$$

The “constants” in the two mass balance equations above depend on the given concentration of MDEA and CO₂ loading in the aqueous solution, respectively. The concentrations of all species can be calculated by solving Equations (6) through (13).

To account for the non-ideality of the solution, in the present study, the Deshmukh-Mather model is used to evaluate the activity coefficient for the species in the MDEA/CO₂/H₂O solution:²⁰

$$\ln \gamma_i = -\frac{AZ_i^2 \sqrt{I}}{1 + B\sqrt{I}} + 2 \sum \beta_{i,j} c_j \quad (14)$$

where γ_i is the activity coefficient for species i in the solution used to correct the concentration of species c_i . The first term on the right-hand side (rhs) is based on the Debye-Huckel theory, which accounts for the contribution from the electrostatic forces among all ions in solution. Z_i is the electrical charge of ion i ; B equals 1.2; I is the ionic strength of the solution; A is taken as a function of temperature as proposed by Lewis.²¹ The second term on the rhs expresses the contribution from short-range interaction forces among species in the solution. β_{ij} are the interaction parameters between the different species i and j in the solution.

To verify the speciation model, CO₂ loading and pH measurements were conducted at different CO₂ partial pressures from 0.05 bar to 1.0 bar. The work was carried out in a 2 L glass cell with 50 wt% MDEA at 50°C. The CO₂ loading was measured by the methanolic potassium hydroxide (KOH) titration method.²² The pH electrode and meter were calibrated at the testing temperature (50°C) with pH 7 and 10 buffer solutions.

CORROSION MODEL FOR CARBON STEEL IN A MDEA/CO₂/H₂O SYSTEM

The corrosion model was based on describing the electrochemical process taking place at the steel surface exposed to a MDEA/CO₂/H₂O environment, as schematically illustrated in Figure 1.

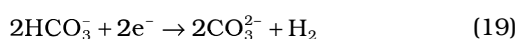
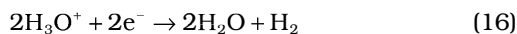
As shown in Figure 1, the electrochemical reactions occurring simultaneously at the steel surface

are dissolution of iron and reduction of the various "oxidizing agents."

Anodic (oxidation) reaction:



Cathodic (reduction) reactions:



Since MDEA/CO₂/H₂O solution under the absorber condition is alkaline (close to pH 9), it can be shown that the contributions of H₃O⁺ reduction and H₂CO₃ reduction reactions are quite small because of the very low concentrations in solution, when compared to other species. In addition, H₂O reduction kinetics is very slow;²³ therefore, it was not considered in the present corrosion model. So, only HCO₃⁻ and MDEAH⁺ reduction reactions (19 and 20) were considered as the key cathodic reactions in this system.

The rates of the electrochemical reactions at the steel surface depend on the electrical potential of the surface, the surface concentrations of species involved in the reactions and temperature. Since electrochemical reactions involve exchange of electrons, the reaction rate can be expressed conveniently as a rate at which the electrons are "consumed or released" (i.e., in terms of an electrical current density, *i*). Fundamental rate equations of electrochemistry relate *i* to the potential at the steel surface (*E*), via an exponential relationship:²⁴

$$i = i_0 \times 10^{\pm \frac{E - E_{\text{rev}}}{b}} \quad (21)$$

which can be written down for each of the electrochemical reactions involved in the corrosion process. The positive sign applies for the anodic reaction while the negative sign applies for the cathodic reactions. The exchange current density is *i*₀, *E*_{rev} is the reversible potential, and *b* is the Tafel slope. In most cases, *i*₀ and *E*_{rev} are nonlinear functions of the surface concentration of species involved in a particular reaction, while all three parameters are functions of temperature.

The model requires as input pH, HCO₃⁻ concentration, and MDEAH⁺ concentration, which can be calcu-

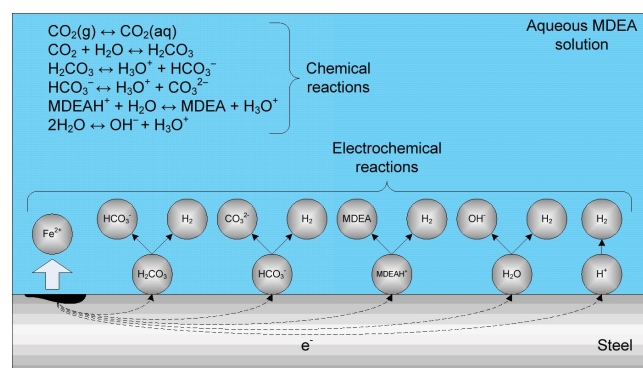


FIGURE 1. Schematic of corrosion process in MDEA-CO₂-H₂O environments.

lated by the thermodynamic speciation model. Once the input parameters are determined, the model calculates cathodic (HCO₃⁻ and MDEAH⁺) and anodic (Fe) current densities with different potentials, and generates a graph with the individual and total cathodic and anodic curves. The intersection of the total cathodic curve with the anodic curve gives the corrosion potential (*E*_{corr}) by solving:²⁵

$$i_{\text{Fe}} = i_{\text{HCO}_3^-} + i_{\text{MDEAH}^+} \quad (22)$$

Corrosion current density (*i*_{corr}) is calculated from the anodic curve (Equation [21]) and the known *E*_{corr}. Finally, the corrosion rate is then recovered by using Faraday's law. If the unit A/m² is used for the corrosion current density, then conveniently the corrosion rate for carbon steel expressed in mm/y takes almost the same numerical value, precisely CR = 1.155 × *i*_{corr}.

The specimens were made of carbon steel (ASTM⁽¹⁾ A36) with a chemical composition of 0.23% C, 0.79% Mn, 0.02% P, 0.03% S, 0.29% Cu, 0.20% Si, and balance Fe. The specimens were ground with 600 grit silicon carbide (SiC) paper, cleaned with isopropyl alcohol (C₃H₈O) in an ultrasonic bath, and dried prior to exposure. Corrosion tests were carried out in a 2 L glass cell at 50°C under atmospheric pressure. Further details of the experimental setup can be found elsewhere.²⁶ To determine electrochemical parameters for anodic and cathodic reactions, potentiodynamic polarization tests were performed in different solutions. Solutions with different HCO₃⁻ concentrations were prepared with sodium bicarbonate (NaHCO₃; 0.5, 1.0, and 1.5 mol/L), and pH was adjusted by addition of solid sodium carbonate (Na₂CO₃). For solutions with different concentrations of MDEAH⁺ at pH 9.1, the concentration of MDEA in each case was calculated in the same way as for a buffer solution (Reaction [4]). The solution was purged with nitrogen (N₂) for 6 h before the experiment and kept purging during the experiment.

For the model verification, an aqueous solution of MDEA with a concentration of 50% by weight was pre-

⁽¹⁾ ASTM International, 100 Barr Harbor Drive, West Conshohocken, PA 19428.

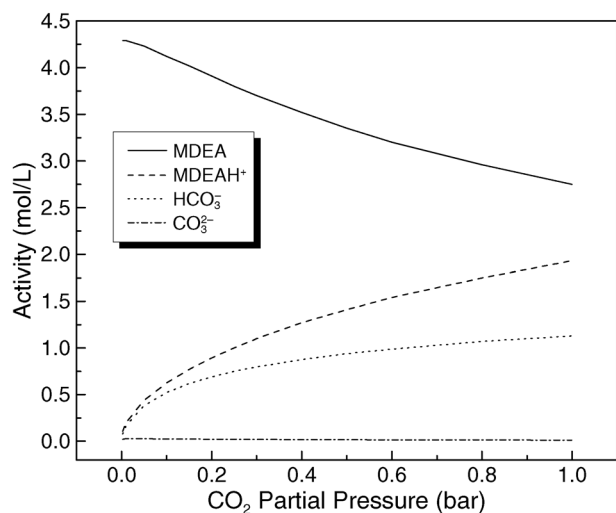


FIGURE 2. Activity of species in 50% MDEA system at 50°C as a function of partial pressure of CO_2 .

pared from a 99% pure MDEA reagent and deionized (DI) water. The test solution was purged with 12% CO_2 gas ($p_{\text{CO}_2} = 0.12$ bar: CO_2 loading = 0.13 mol CO_2 /mol amine).

The corrosion rate of carbon steel for each condition was measured by linear polarization resistance (LPR) method. LPR measurements were performed within ± 10 mV with respect to the corrosion potential with a scan rate of 0.166 mV/s. The potentiodynamic polarization tests were carried out after conducting LPR measurements. The specimen was scanned potentiodynamically at a rate of 0.166 mV/s from the corrosion potential to either anodic or cathodic directions.

RESULTS AND DISCUSSION

Figure 2 shows the activity (which is defined as the activity coefficient $[\gamma_i]$ times concentration $[c_i]$) for the species in a 50 wt% MDEA system at 50°C at different CO_2 partial pressures. As shown in Figure 2, activities of MDEA and CO_3^{2-} decreased with CO_2 partial pressure whereas they increased for MDEAH⁺ and HCO_3^- .

The calculated pH of 50 wt% MDEA solution at 50°C under different CO_2 partial pressures is compared with the measurements in Figure 3. The comparison of the calculated CO_2 loading as a function of partial pressure of CO_2 with our own and open literature²⁷ data is shown in the same figure. There it can be seen that the speciation model performs reasonably well.

The electrochemical parameters for the reactions that were considered in the present study are summarized in Tables 1 and 2. They were found in the open literature²⁴⁻²⁵ and determined from the electrochemical data obtained in the present study. It is important

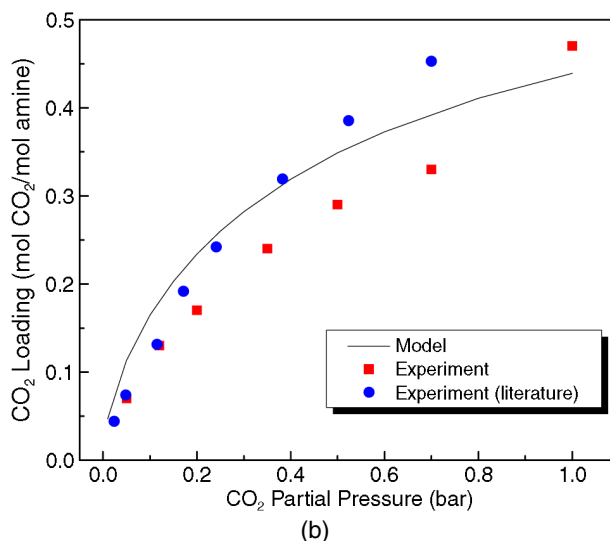
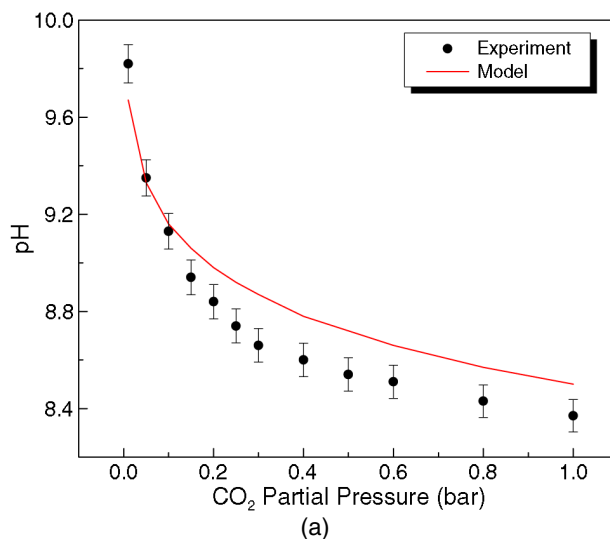


FIGURE 3. Comparison between experimental data²⁷ and calculations: (a) pH and (b) CO_2 loading at different CO_2 partial pressures (50% MDEA system at 50°C).

to note that mass-transfer effect is not included in the present model because of the high concentration of oxidizing agents (HCO_3^- and MDEAH⁺), which suggests that those are involved in the charge-transfer-controlled reduction reaction.²³ Furthermore, in the follow-up electrochemical work it was confirmed that HCO_3^- and MDEAH⁺ reduction reactions are under charge-transfer control.

Determination of Reaction Order

• **Iron Dissolution** — To determine reaction orders with respect to HCO_3^- and H^+ for iron dissolution reaction, polarization tests were conducted under different test conditions shown in Table 3.

Figure 4 shows the anodic polarization curves of carbon steel at different HCO_3^- concentrations. It can be seen clearly that anodic current density increased and corrosion potential decreased with increasing HCO_3^- concentration. Figure 5 is a plot of the log of the

TABLE 1
Electrochemical Parameters for the Exchange Current Density Included in the Model

	i_o (A/m ²)	$i_{o,ref}$ (A/m ²)	$C_{H^+,ref}$ (molar)	$C_{HCO_3^-,ref}$ (molar)	$C_{MDEAH^+,ref}$ (molar)
Fe oxidation (15)	$i_{o,Fe} = i_{o,Fe,ref} \left(\frac{C_{HCO_3^-}}{C_{HCO_3^-,ref}} \right)^\alpha \left(\frac{C_{H^+}}{C_{H^+,ref}} \right)^\beta$	0.53	$10^{-9.1}$	1	—
HCO ₃ ⁻ reduction (19)	$i_{o,HCO_3^-} = i_{o,HCO_3^-,ref} \left(\frac{C_{HCO_3^-}}{C_{HCO_3^-,ref}} \right)^\delta$	0.15	—	0.5	—
MDEAH ⁺ reduction (20)	$i_{o,MDEAH^+} = i_{o,MDEAH^+,ref} \left(\frac{C_{MDEAH^+}}{C_{MDEAH^+,ref}} \right)^\kappa$	0.15	—	—	0.63

current density at constant potential (-0.74 V) vs. the log of the concentration of HCO₃⁻ at pH 9.1. The slope is 1.86, indicating that the reaction order (α) is close to 2. Figure 6 shows the measured anodic polarization curves and the calculated Tafel lines at different HCO₃⁻ concentrations. The Tafel lines were produced with the reaction order of 2 and the Tafel slope of 0.12 V/decade. A reasonable agreement is seen, considering that there is very little linearity in the measured curves, which is likely from the passivation of the steel surface caused by polarization.

Figure 7 shows the anodic polarization curves of carbon steel at different pH values. The anodic current density increased and the corrosion potential decreased with increasing pH. Figure 8 is a plot of the log of the current density at constant potential (-0.7 V) vs. the log of the pH. The slope of the plot showed a slope of approximately -0.5, indicating the reaction order (β). Figure 9 shows the measured anodic polarization curves and the calculated Tafel lines at different pH. The Tafel lines were produced with the reaction order of -0.5 and the Tafel slope of 0.12 V/decade. Again, the agreement can be considered being reasonable considering the nonlinearity of the experimental curves as a result of passivation.

Based on the results presented above, reaction orders of HCO₃⁻ and H⁺ for iron dissolution reaction were determined as:

$$i_{o,Fe} = i_{o,Fe,ref} \left(\frac{C_{HCO_3^-}}{C_{HCO_3^-,ref}} \right)^2 \left(\frac{C_{H^+}}{C_{H^+,ref}} \right)^{-0.5} \quad (23)$$

• Bicarbonate Reduction — To determine the reaction order for the HCO₃⁻ reduction reaction (Reaction [19]), cathodic polarization tests were conducted using a range of test conditions as shown in Table 4.

Figure 10 shows the cathodic polarization curves of carbon steel at different HCO₃⁻ concentrations at pH 9.1. The cathodic current density slightly increased and the corrosion potential decreased with increas-

TABLE 2

Electrochemical Parameters for the Reversible Potential and Tafel Slope Included in the Model

	E_{rev} (V)	b (V)
Fe oxidation (15)	$E_{rev} = E_{o,Fe^{2+}/Fe} + \frac{2.3RT}{2F} \log c_{Fe^{2+}}$	0.12
HCO ₃ ⁻ reduction (19)	$E_{rev} = -\frac{2.3RT}{F} \text{pH}$	$b = \frac{2.3RT}{0.5F}$
MDEAH ⁺ reduction (20)	$E_{rev} = -\frac{2.3RT}{F} \text{pH}$	$b = \frac{2.3RT}{0.5F}$

TABLE 3

Test Conditions for Determining Iron Dissolution Reaction Orders

Solutions	HCO ₃ ⁻ Concentration (mol/L)		pH	Temperature (°C)
α NaHCO ₃ /Na ₂ CO ₃ /H ₂ O	0.5, 1.0, 1.5		9.1	50
β NaHCO ₃ /Na ₂ CO ₃ /H ₂ O	1.0		7, 8, 9	50

ing HCO₃⁻ concentration. Figure 11 is a plot of the log of the current density at constant potential (-0.95 V) vs. the log of the concentration of HCO₃⁻. The slope of the line in the plot is 0.39, indicating that the reaction order (δ) is close to 0.5. Figure 12 shows the measured cathodic polarization curves and the calculated Tafel lines at different HCO₃⁻ concentrations. The Tafel lines were produced with the reaction order of 0.5 and the Tafel slope of 0.128 V/decade. A reasonable agreement between experimental polarization curves and calculated Tafel lines is seen, although one can argue that this effect is within the margins of experimental error. Based on these results, the reaction order for HCO₃⁻ reduction reaction was determined as:

$$i_{o,HCO_3^-} = i_{o,HCO_3^-,ref} \left(\frac{C_{HCO_3^-}}{C_{HCO_3^-,ref}} \right)^{0.5} \quad (24)$$

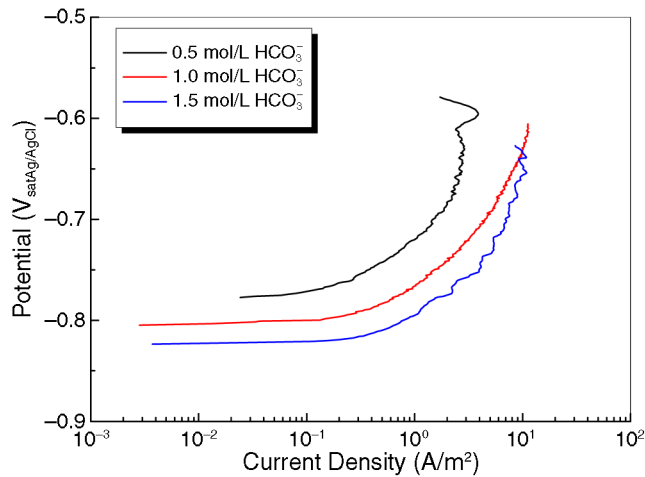


FIGURE 4. Anodic polarization curves for carbon steel at different HCO_3^- concentrations.

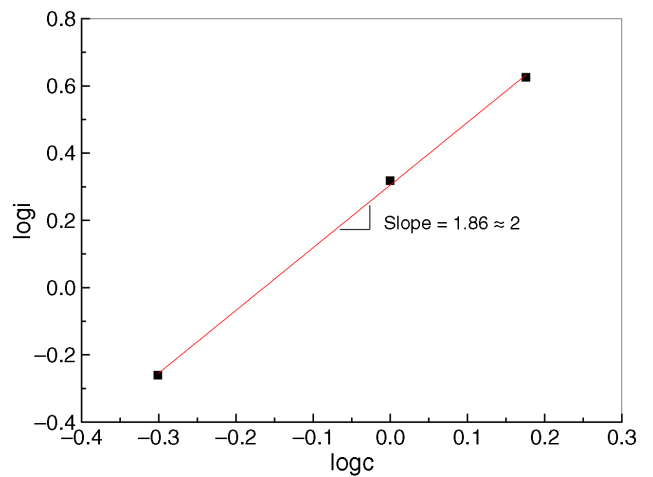


FIGURE 5. Determination of iron dissolution reaction order with regard to HCO_3^- concentration.

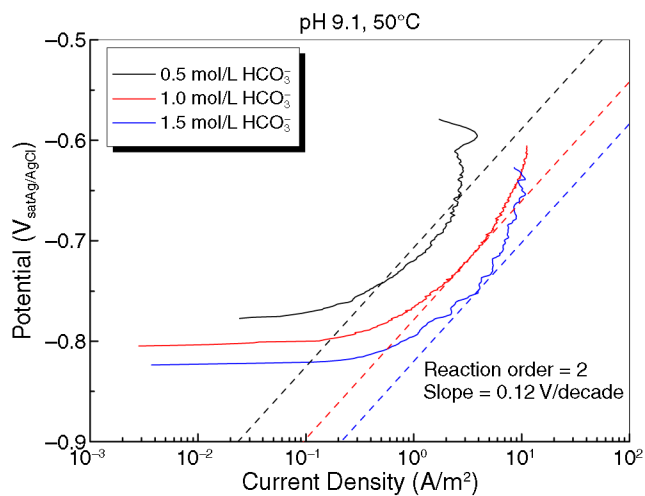


FIGURE 6. Measured anodic polarization curve and calculated Tafel lines for iron dissolution at different HCO_3^- concentrations.

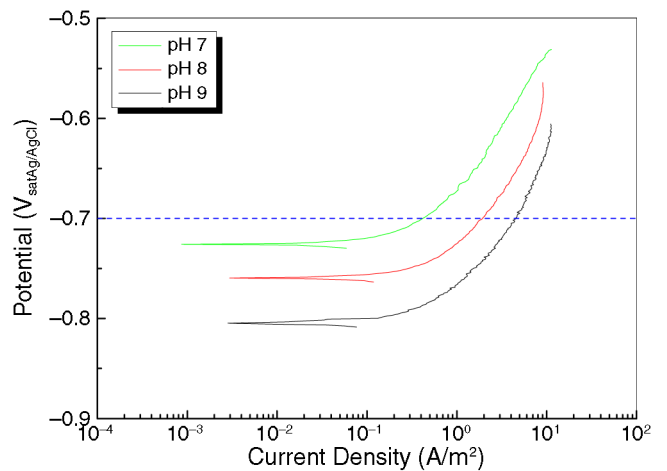


FIGURE 7. Anodic polarization curves of carbon steel at different pH.

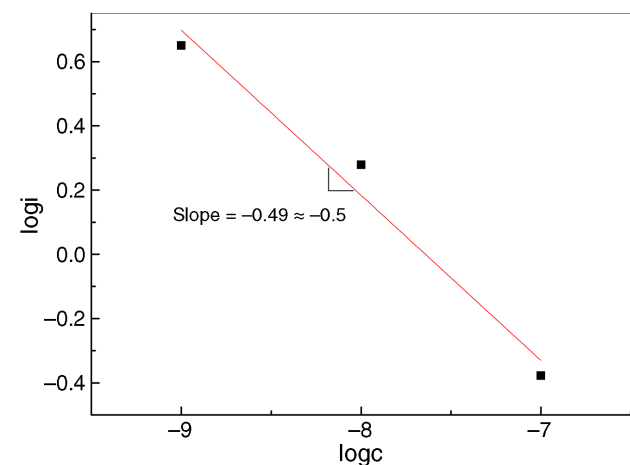


FIGURE 8. Determination of the iron dissolution reaction order with regard to H^+ concentration.

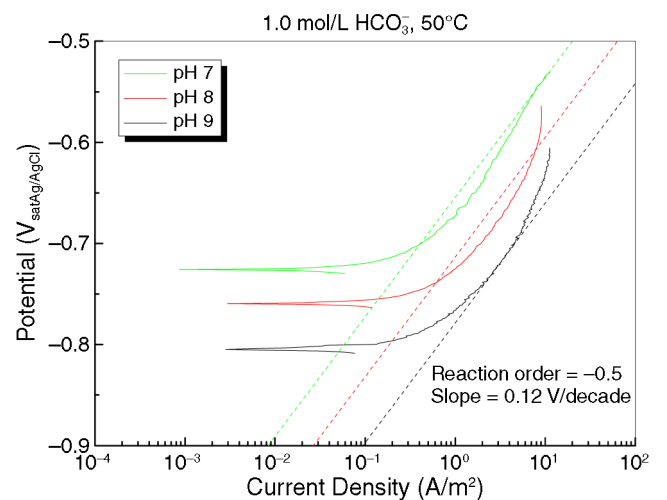


FIGURE 9. Measured anodic polarization curves and calculated iron Tafel lines for dissolution at different pH.

TABLE 4

Test Conditions for Determining the HCO_3^- Reduction Reaction Order

Solutions	HCO_3^- Concentration (mol/L)	pH	Temperature ($^{\circ}\text{C}$)
δ $\text{NaHCO}_3/\text{Na}_2\text{CO}_3/\text{H}_2\text{O}$	0.5, 1.0, 1.5	9.1	50

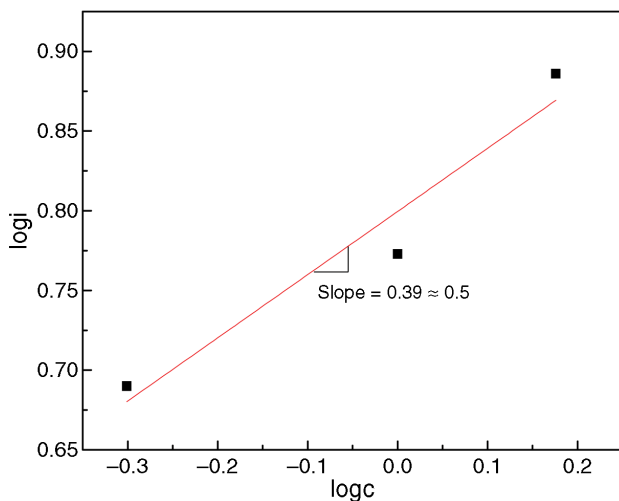
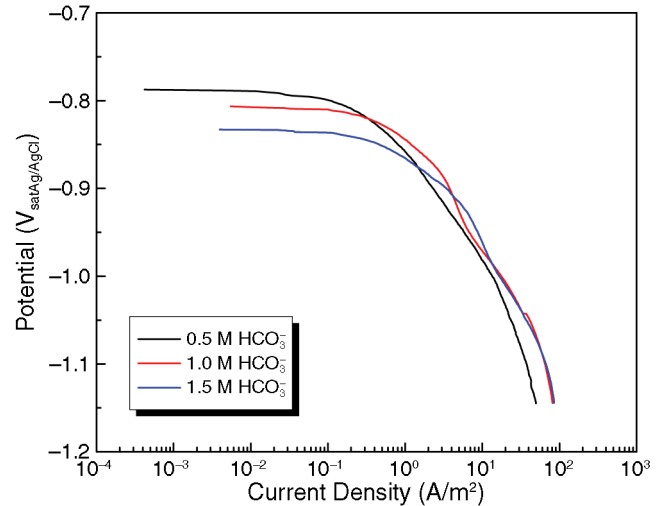
• Protonated MDEA Reduction — To determine the reaction order for the MDEAH^+ reduction reaction (Reaction [20]), cathodic polarization tests were conducted at different test conditions shown in Table 5.

Figure 13 shows the cathodic polarization curves for carbon steel at different MDEAH^+ concentrations at pH 9.1. The cathodic current density increased with increasing MDEAH^+ concentration. Figure 14 is a plot of the log of the current density at constant potential (-0.8 V) vs. the log of the concentration of MDEAH^+ . The slope of the line in the plot is approximately 1.3, indicating that the reaction order (κ) is close to 1. Figure 15 shows the comparison of the measured cathodic polarization curves and the calculated Tafel lines at different MDEAH^+ concentrations. The Tafel lines were produced with the reaction order of 1 and the Tafel slope of 0.128 V/decade. A good agreement between the experimental polarization curve and the calculated Tafel line at different MDEAH^+ concentrations is seen.

Based on these results, a reaction order for MDEAH^+ reduction reaction was determined as:

$$i_{o,\text{MDEAH}^+} = i_{o,\text{MDEAH}^+,\text{ref}} \left(\frac{c_{\text{MDEAH}^+}}{c_{\text{MDEAH}^+,\text{ref}}} \right)^1 \quad (25)$$

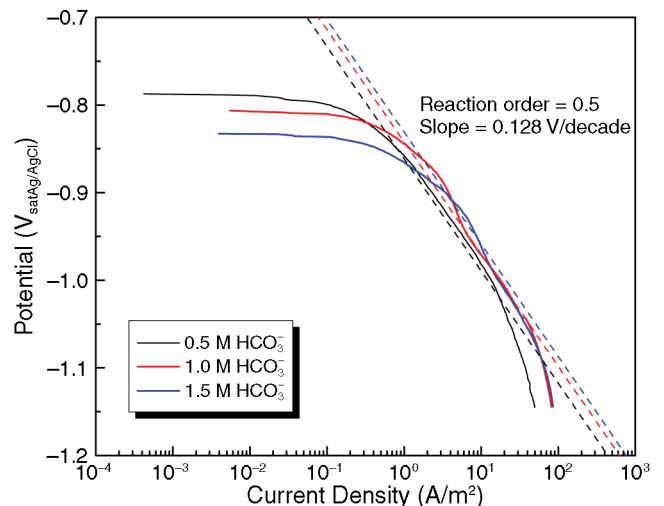
Validation of the Overall Corrosion Model — Performance of the overall corrosion model was validated

**FIGURE 11.** Determination of the reaction order for HCO_3^- reduction.**FIGURE 10.** Cathodic polarization curves for carbon steel at different HCO_3^- concentrations.**TABLE 5**

Test Conditions for Determining the Reaction Order for MDEAH^+ Reduction

Solutions	HCO_3^- Concentration (mol/L)	pH	Temperature ($^{\circ}\text{C}$)
κ $\text{MDEA}/\text{HCl}/\text{H}_2\text{O}$	0.33, 0.63, 1	9.1	50

by comparing the predictions with results from experiments. Figure 16 compares corrosion rates between experiment and prediction at different HCO_3^- concentrations and pH. The predicted corrosion rates showed good agreement with experimental data with an error not larger than 20% to 30%, which can be considered to be within the experiential error range for the current LPR measurements.

**FIGURE 12.** Measured cathodic polarization curve and calculated Tafel lines for HCO_3^- reduction at different HCO_3^- concentrations.

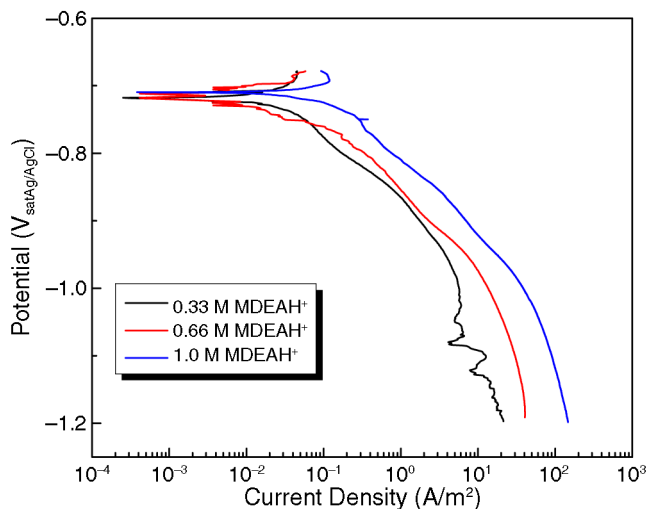


FIGURE 13. Cathodic polarization curves for carbon steel at different MDEAH⁺ concentrations.

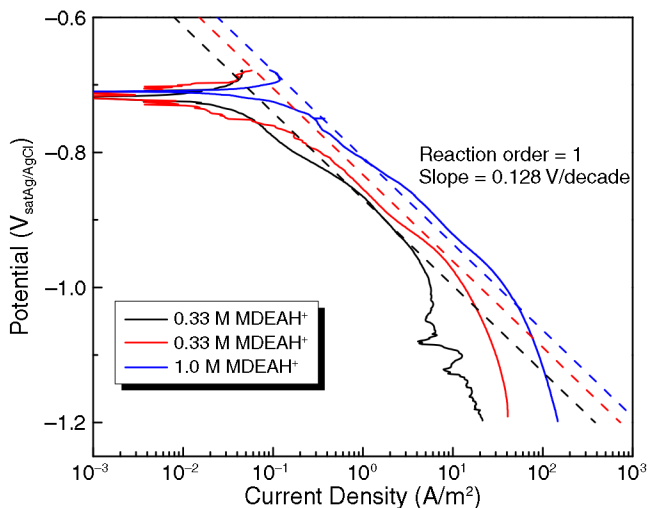


FIGURE 15. Measured cathodic polarization curves and calculated Tafel lines for MDEAH⁺ reduction at different MDEAH⁺ concentrations.

Figure 17 shows the comparison of experimental and calculated polarization curves²⁶ and corrosion rates for a 50 wt% MDEA/12% CO₂ condition. Although predicted polarization curves indicate a higher corrosion potential than seen in the experiments, given the complexity of the system, one can accept this result, particularly in light of the reasonable agreement of the corrosion current/rate, as shown in Figure 17. Many similar comparisons were made for other conditions covered in this study, with similar results. This indicates that the current corrosion model is applicable to uniform corrosion of carbon steel in the absorber conditions if there is no major deviation from the conditions studied here: MDEA concentration (50 wt%) and temperature (50°C). Further work is ongoing to extend the validity of the model to cover a broader range of conditions such as those seen in the regenerator.

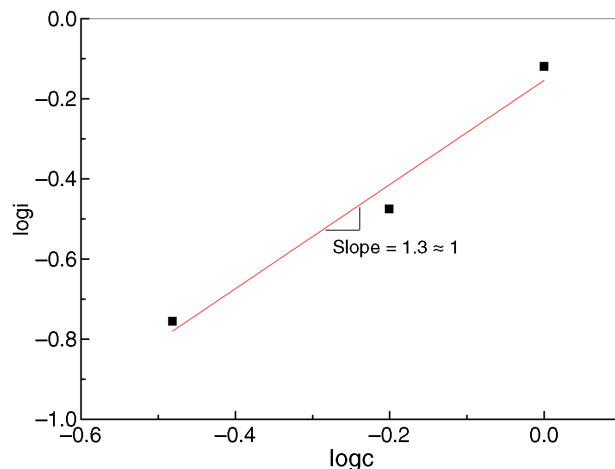


FIGURE 14. Determination of the reaction order for MDEAH⁺ reduction.

CONCLUSIONS

A predictive model was developed for corrosion of carbon steel in CO₂-loaded aqueous MDEA systems based on modeling of solution speciation and electrochemical reactions. The following conclusions were drawn:

- ❖ Activities of MDEA and CO₃²⁻ decreased with CO₂ partial pressure whereas they increased with CO₂ partial pressure for MDEAH⁺ and HCO₃⁻.
- ❖ The speciation model showed a good agreement with experimental data for pH and CO₂ loading.
- ❖ The required electrochemical parameters (e.g., exchange current densities, Tafel slopes, and reaction orders) for the Fe dissolution, HCO₃⁻ reduction, and MDEAH⁺ reduction reactions were determined by experiments and used successfully to build a corrosion model for corrosion of carbon steel in MDEA/CO₂/H₂O environments.
- ❖ The corrosion model showed a good agreement with experimental data for various environmental conditions including pure CO₂ and MDEA/CO₂ solutions.

ACKNOWLEDGMENTS

The authors would like to acknowledge the financial support from Alstom Power Inc. to the Institute for Corrosion and Multiphase Technology at Ohio University on this project.

REFERENCES

1. E. Fleury, J. Kittel, B. Vuillemin, R. Oltra, F. Ropital, "Corrosion in Amine Units for Acid Gas Treatment: A Laboratory Study," EUROCORR 2009, paper no. SS 12-O-7888 (Frankfurt, Germany: Dechema e.V. 2009).
2. W. Tanthapanichakoon, A. Veawab, B. McGarvey, *Ind. Eng. Chem. Res.* 45 (2006): p. 2586.
3. W. Liu, D. King, J. Liu, B. Johnson, Y. Wang, Z. Yang, *JOM* 61 (2009): p. 36.
4. M.R. Khorrami, K. Raeissi, H. Shahban, M.A. Torkan, A. Saatchi, *Corrosion* 64 (2008): p. 124.

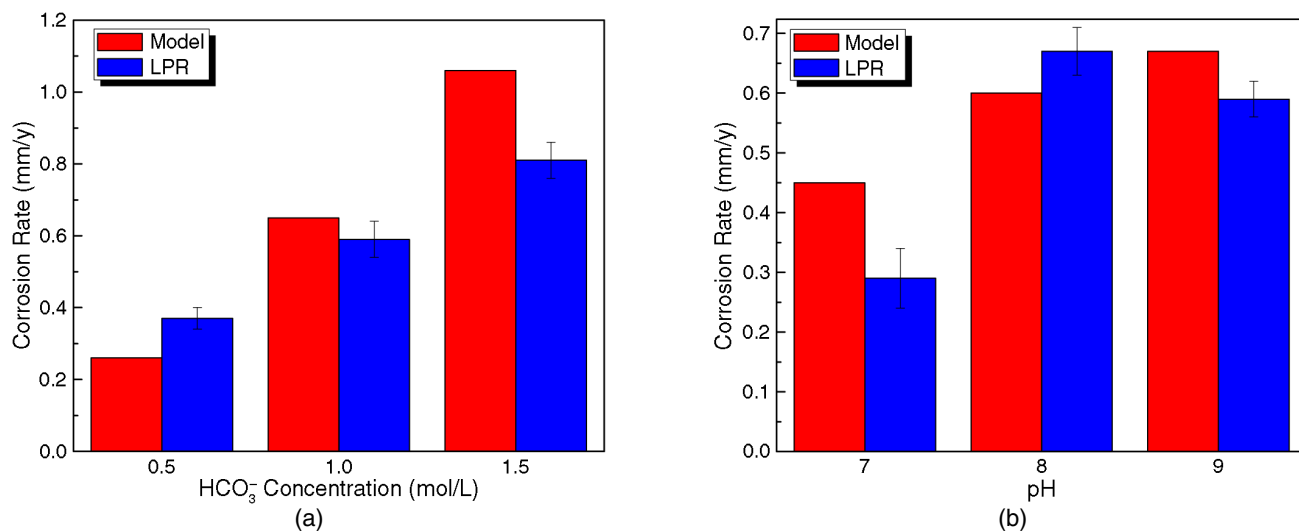


FIGURE 16. Comparison of corrosion rates between experiments and predictions at different conditions: (a) at different HCO_3^- concentrations and (b) at different pH.

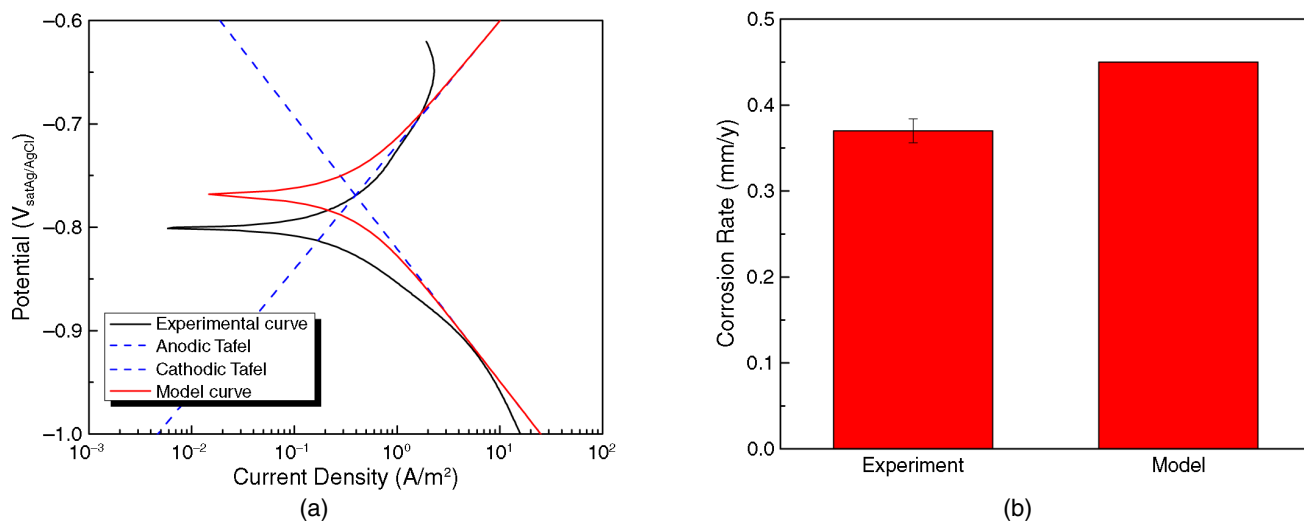


FIGURE 17. Comparison between experimental data and predictions in a 50 wt% MDEA/12% CO_2 system at 50°C: (a) polarization curves and (b) corrosion rates.

- M.S. DuPart, T.R. Bacon, D.J. Edwards, *Hydrocarb. Process.* (1993): p. 89.
- Y. Tomoe, M. Shimizu, H. Kaneta, "Active Dissolution and Natural Passivation of Carbon Steel in Carbon Dioxide-Loaded Alkanolamine Solutions," CORROSION/96, paper no. 395 (Houston, TX: NACE International, 1996).
- X.-P. Guo, Y. Tomoe, *Corros. Sci.* 41 (1999): p. 1391.
- A. Veawab, P. Tontiwachwuthikul, A. Chakma, *Ind. Eng. Chem. Res.* 38 (1999): p. 3917.
- M. Nainar, A. Veawab, *Ind. Eng. Chem. Res.* 48 (2009): p. 9299.
- A. Veawab, P. Tontiwachwuthikul, A. Chakma, *Ind. Eng. Chem. Res.* 40 (2001): p. 4771.
- W. Tanthapanichakoon, A. Veawab, *Corrosion* 61 (2005): p. 371.
- S. Rennie, *Mater. Forum* 30 (2006): p. 126.
- A. Veawab, A. Aroonwilas, *Corros. Sci.* 44 (2002): p. 967.
- F. Camacho, S. Sanchez, R. Pacheco, M.D. La Rubia, A. Sanchez, *Int. J. Chem. Kinet.* 41 (2009): p. 204.
- D.M. Austgen, G.T. Rochelle, C.-C. Chen, *Ind. Eng. Chem. Res.* 30 (1991): p. 543.
- R.H. Weiland, T. Chakravarty, A.E. Mather, *Ind. Eng. Chem. Res.* 32 (1993): p. 1419.
- E.T. Hessen, T.H. Warberg, H.F. Svendsen, *Energy Procedia* 1 (2009): p. 971.
- A. Vrachnos, G. Kontogeorgis, E. Voutsas, *Ind. Eng. Chem. Res.* 45 (2006): p. 5148.
- H.A. Al-Ghawas, D.P. Hagewiesche, G. Ruiz-Ibanez, O.C. Sandall, *J. Chem. Eng. Data* 34 (1989): p. 385.
- A. Benamor, M.K. Aroua, *Fluid Phase Equilibria* 231 (2005): p. 150.
- G.N. Lewis, *Thermodynamics*, 2nd ed. (New York, NY: McGraw-Hill Book Company, 1961), p. 640.
- R. Notz, H.P. Mangalapally, H. Hasse, *Int. J. Greenhouse Gas Control* 6 (2012): p. 84.
- L.G.S. Gray, B.G. Anderson, M.J. Danysh, P.R. Tremaine, "Effect of pH and Temperature on the Mechanism of Carbon Steel Corrosion by Aqueous Carbon Dioxide," CORROSION/90, paper no. 40 (Houston, TX: NACE, 1990).
- M. Nordsveen, S. Nešić, R. Nyborg, A. Stangeland, *Corrosion* 59 (2003): p. 443.
- S. Nešić, J. Postlethwaite, S. Olsen, *Corrosion* 52 (1996): p. 280.
- Y.S. Choi, D. Duan, S. Nešić, F. Vitse, S.A. Bedell, C. Worley, *Corrosion* 66 (2010): p. 125004.
- M.K. Park, O.C. Sandall, *J. Chem. Eng. Data* 46 (2001): p. 166.